文章编号：1001-9014(2021)01-0007-06
DOI:10. 11972/j. issn. 1001-9014. 2021. 01. 002

Reducing V_{oc} loss in InGaAsP/InGaAs dual-junction solar cells

LU Hong-Bo[1,2,3], LI Xin-Yi[2*], LI Ge[2], ZHANG Wei[2], HU Shu-Hong[1], DAI Ning[1*], YANG Gui-Ting[2]

(1. State Key Laboratory of Infrared Physics, Shanghai Institute of Technology Physics of the Chinese Academy of Sciences, Shanghai 200083, China;
2. State Key Laboratory of Space Power-sources, Shanghai Institute of Space Power-sources, Shanghai 200245, China;
3. University of Chinese Academy of Sciences, Beijing 100049, China)

Abstract: Smaller V_{oc} of 1. 0 eV/0. 75 eV InGaAsP/InGaAs double-junction solar cell (DJSC) than the V_{oc} sum of individual subcells has been observed, and there is little information of the origin of such V_{oc} loss and how to minimize it. In this paper, it is disclosed that the dominant mechanism of minority-carrier transport at back-surface-field (BSF)/base interface of the bottom subcell is thermionic emission, instead of defect-induced recombination, which is in contrast to previous reports. It also shows that both InP and InAlAs cannot prevent the zinc diffusion effectively. In addition, intermixing of major III-V element occurs as a result of increasing thermal treatment. To suppress the above negative effects, an initial novel InP/InAlAs superlattice (SL) BSF layer is then proposed and employed in bottom InGaAs subcell. The V_{oc} of fabricated cells reach 997. 5 mV, and a reduction of 30 mV in *Voc* loss without lost of *Jsc*, compared with the results of conventional InP BSF configuration, is achieved. It would benefit the overall V_{oc} for further four-junction solar cells.

Key words: Back-surface field, InGaAsP/InGaAs dual-junction, open-circuit voltage, superlattice.
PACS: 88. 40. jp, 78. 67. HC, 75. 40. Mg

InGaAsP/InGaAs双结太阳电池的开路电压损耗抑制

陆宏波[1,2,3]，李欣益[2*]，李 戈[2]，张 玮[2]，胡淑红[1]，戴 宁[1*]，杨瑰婷[2]
(1. 中国科学院上海技术物理研究所,红外物理国家重点实验室,上海 200083;
2. 上海空间电源研究所,空间电源技术国家重点实验室,上海 200245;
3. 中国科学院大学,北京 100049)

摘要:现有1.0 eV/0.75 eV InGaAsP/InGaAs双结太阳电池的开路电压小于各子电池的开路电压之和,鲜有研究探索开路电压损耗的来源以及如何抑制。通过研究发现,InGaAs底电池背场/基区界面处的少数载流子输运的主要机制是热离子发射,而不是缺陷诱导复合。SIMS测试表明,采用InP或InAlAs背场均不能有效抑制Zn掺杂剂的扩散。此外,由于生长过程中持续的高温热处理,III-V族主元素在界面处发生了热扩散。为了抑制上述现象,提出了一种新型InP/InAlAs超晶格背场,并应用到InGaAs底电池中。制备得到的双结太阳电池在维持短路电流密度不变的情况下,开路电压提升到997.5 mV,与传统采用InP背场的双结太阳电池相比,开路电压损耗降低了30 mV。该研究成果对提升四结太阳电池的整体开路电压有重要意义。

关 键 词:背场;InGaAsP/InGaAs双结电池;开路电压;超晶格
中图分类号:TM914.4　　**文献标识码**:A

Introduction

InGaAsP/InGaAs double-junction solar cells (DJSCs) with approximate bandgap combination of 1. 0/0. 75 eV are used in four-junction configuration to harvest 900~1 700 nm sunlight, and are crucially important for device performances [1]. Previous reports Ref. [2-4]

Received date: 2020- 04- 16, **revised date**: 2020- 06- 05　　**收稿日期**:2020- 04- 16,**修回日期**:2020- 06- 05
Foundation items: Supported by the National Nature Science Foundation of China (61474076 and 61704106), the Young Elite Scientist Sponsorship Program by China Association for Science and Technology (2017QNRC001) and Shanghai Rising-Star Program (18QB1402500 and 19QB1403800).
Biography: Lu Hong-Bo, male, Shanghai, master. Research area involves III-V Semiconductor materials and devices. E-mail: lhb2139@163. com.
* **Corresponding author**: E-mail: lixy_sisp@163. com

show that open-circuit voltage (V_{oc}) of InGaAsP/InGaAs DJSC is smaller than the sum of individual subcells. To evaluate solar cells with different bandgaps, bandgap-voltage offset under open-circuit condition (W_{oc}) is introduced [5]. For multijunction solar cells, *Woc* can be described as

$$W_{oc}(J_{sc}) = \frac{1}{q}\left[\sum_i E_g^i - V_{oc}\left(J_{sc}\right)\right] \quad , \quad (1)$$

where E_g^i is the bandgap of each subcell, and $V_{oc}(Jsc)$ stands for the open-circuit voltage when the device produces a given value of short-circuit current (Jsc) under illumination. And the V_{oc} loss for multijunction solar cells would be defined as the gap between W_{oc}^m and the sum of W_{oc}^i of subcells, as $W_{oc}^m - \sum_i W_{oc}^i\left(J_{sc}\right)$.

W_{oc}^m of InGaAsP/InGaAs DJSC at Jsc of conventional four-junction configuration (about 16.5 mA/cm^2) is above 820 mV, higher than the W_{oc} sum of InGaAsP (~330 mV) and InGaAs (~340 mV) individual subcells. Part results from previous reports are listed in Table 1, and there is no reference reporting the origin of such V_{oc} loss and how to minimize it.

Experience on III-V semiconductor devices reveals that the diffusion and intermixing at heterojunction interface of InP system always leads to device performance degradation[6]. Moreover, from the viewpoint of physics of solar cell device, the V_{oc} of solar cells majorly depends on the heterojunction interface between base and back-surface field (BSF) layers. Therefore, considering the thermal history of DJSC structure, the bottom InGaAs subcell, especially the BSF/base interface, might be the key role to reduce V_{oc} loss.

In this paper, the evolution of dopant diffusion and recombination at BSF/base interface with increasing thermal treatment is studied. Based on experimental results, we propose a novel InP/InAlAs superlattice (SL) BSF layer for bottom InGaAs subcell. A reduction of 30 mV in V_{oc} loss is achieved, compared with the results of conventional InP BSF configuration. It shows that such SL BSF would benefit the V_{oc} enhancement for four-junction solar cells.

1 Experiments

Growth are done on *n*-type <100> InP substrates using MOVPE technique. The primary group III and group V precursors used are trimethylgallium (TMGa), trimethylindium (TMIn), trimethylgallium (TMAl), arsine (AsH_3), and phosphine (PH_3). The dopant precursors used are silane (SiH_4) and diethylzinc (DEZn). V/III ratio of 200~300 and growth temperature of 650 °C are employed, as described previously [7].

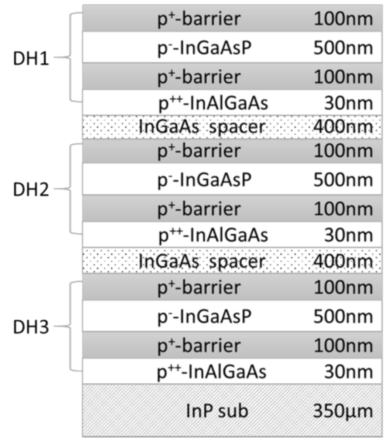

Fig. 1 Cross-section of MOVPE stack containing three BSF/InGaAsP/BSF DHs.
图1 含3对BSF/InGaAsP/BSF双异质结结构样品示意图

Three periods of isotype p^+-barrier (100nm)/p^--InGaAsP (500nm)/p^+-barrier (100nm)/p^{++}-In ($Al_{0.1}Ga_{0.9}$) As (100nm) double heterojunctions (DHs), separated by InGaAs spacer layers, are grown in the same stack of MOVPE layers, as illustrated in Fig. 1. Two types of barriers, InP and InAlAs respectively, are employed. After growth, individual DHs are exposed by a series of selective etches. Diluted HCl solution and H_2SO_4: H_2O_2: H_2O solution are used for InP layers and arsenide layers, respectively. The overall element profiles in DHs are obtained through secondary ion mass spectra (SIMS) measurement, while the minority-carrier recombination process in DHs are evaluated using time-resolved photoluminescence (TRPL) technique. It should be pointed out that, the bandgap of p^--InGaAsP in DHs is 0.83 eV, for TRPL measurement convenience.

SIMS measurements are performed using Cs^+ primary beam with a fixed 5 kV acceleration. The positive ions of the quasi-molecular cluster are collected and detected. TRPL measurements with a temporal resolution of ~ 200 ps are performed at room temperature. An H-10330-75 PMT is used to collect PL signals.

The schematic cross-section of InGaAsP/InGaAs (1.0/0.75 eV) DJSC structure is shown in Fig. 2. The active region of each subcell consists of *n*-on-*p* junction (emitter/base) surrounded by *n*-type InP window layer and *p*-type BSF layer. In($Al_{0.1}Ga_{0.9}$)As tunnel junction is used to connect subcells. The structures are then processed following the standard III-V solar cell device art.

Table 1 Previous reported results for InGaAsP/InGaAs DJSC
表1 文献报道的InGaAsP/InGaAs双结电池电性能

Reference	Method	Bandgap	Illumination	J_{sc} (mA/cm^2)	V_{oc} (mV)	W_{oc} (mV)
Oshima [2]	MBE	1.0/0.71	AM1.5G	13.1	570	1140
Wu [3]	MBE	1.05/0.73	AM1.5G	16.1	830	950
Zhao [4]	MOVPE	1.07/0.74	AM1.5D	10.2	977	833

The cells are 1.0×1.0 cm^2 in size.

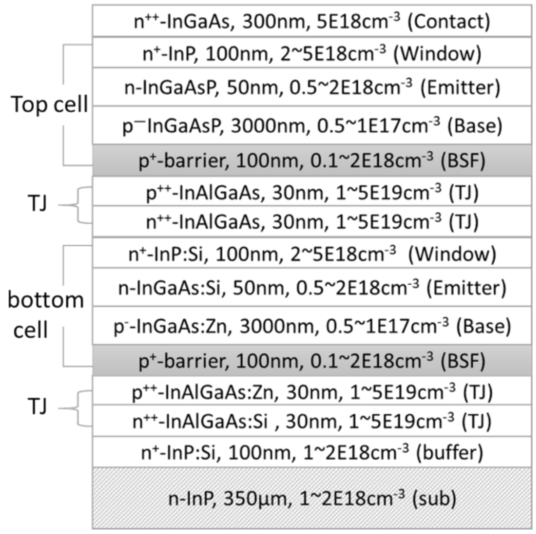

Fig. 2　Cross-section of the InGaAsP/InGaAs double-junction solar cell structure.
图 2　InGaAsP/InGaAs 双结太阳电池结构示意图

In-house photovoltaic current density-voltage (J–V) measurements are performed under AM0 solar simulator, without GaAs filter. External quantum efficiency (EQE) measurements are performed to give qualitative insight into the spectral response. Cells are placed on 25 °C cooled stages during measurements.

2　Results and discussions

Figure 3 shows the element profiles and PL decay curves for topmost DHs (DH1) in InP-barrier and InAlAs-barrier stacks. The zinc concentration around both DH center regions are of the same level about 5-6×10^{16} cm^{-3}, which is similar to the typical doping level of base in solar cells. Sharp zinc diffusion profile near the interface between InGaAsP and barriers is observed. It should be pointed out that, the zinc doping level of both InP and InAlAs layers in DHs have been increased to 1-2×10^{18} cm^{-3}, almost one order of magnitude higher than typical doping level used in BSF layer, to exacerbate such diffusion behavior. Moreover, the zinc concentration in the underneath $In(Al_{0.1}Ga_{0.9})As$ layer reaches 2×10^{19} cm^{-3}. The nearly identical profiles of zinc atom suggest that both InP and InAlAs layer are of the similar effect as anti-diffusion barriers during the growth.

It evidences in Fig. 3 that the minority-carrier decay time in InAlAs-barrier DH is much larger than that in InP-barrier DH. In symmetrical DHs, the effective lifetime τ_{eff} extracted from PL decay is related to both bulk carrier lifetime τ_{bulk} and surface recombination velocity S, as Ref. [8]

$$\frac{1}{\tau_{eff}} = \frac{1}{\tau_{bulk}} + \frac{2S}{d} \quad , \quad (2)$$

where d is the thickness of confined layer in the DH. For high-quality materials, the τ_{bulk} approximately equals to

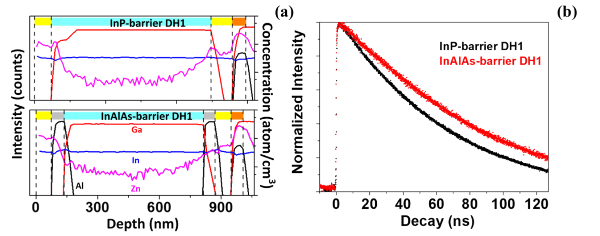

Fig. 3　Element profiles (a) and PL decay curves (b) for InP-barrier and InAlAs-barrier DH1s.
图 3　InP 和 InAlAs 背场双异质结的元素深度剖析(a)和荧光发光衰减曲线(b)

the reciprocal product of spontaneous radiative recombination coefficient B and doping concentration N

$$\tau_{bulk} = (BN)^{-1} \quad . \quad (3)$$

The value of B could be calculated according to Ref. [9]. With the doping concentration acquired from SIMS, the τ_{bulk} in DH1 is about 200 ns. By mono-exponential fitting of decay curves, τ_{eff} of 70 ns and 110 ns are obtained for InP-barrier DH and InAlAs-barrier DH. According to Eq. 2, the experimental S for InP/InGaAsP interface and InAlAs/InGaAsP interface are 232 cm/s and 103 cm/s, respectively. Such small recombination velocity suggests that the radiative process in the bulk dominates the carrier recombination, and the recombination at the interface is nearly neglectable.

The primary mechanism of carrier transport at heterojunction interface includes thermionic emission and defect-induced recombination. When thermionic emission dominates, the recombination current writes [10]

$$J_0 = qSn_1 = q\frac{m_2}{m_1}\left(\frac{2k_BT}{\pi m_1}\right)^{\frac{1}{2}} e^{-\frac{\Delta E}{k_BT}} \cdot n_1 \quad , \quad (4)$$

where m_1 and m_2 are effective mass of confined material and barrier, and ΔE is band offset. It is quite obvious that S would exponentially decreases as the band offset increasing. Notice that electron is the minority-carrier in p-InGaAsP DHs. The values of S for DHs, in the scenario of thermionic emission dominating, are estimated using ΔEc and $m_{1,2}$ from Ref. [11], as listed in Table 2. Surface recombination velocities S of 5793 cm/s and 0.738 cm/s are obtained for InP-barrier DH and InAlAs-barrier DH, respectively. Both calculated and experimental values show that, InAlAs-barrier DH presents smaller surface recombination velocity at heterojunction interface. Consider the complicated carrier transport mechanism at heterojunction interface, the gap between experimental S will not be so large. For example, the sharp diffusion profile of zinc would develop built-in field near the interface, it should reduce the population of minority-carrier reaching the interface and therefore, smaller theoretical value of S could be expected, especially for InP-barrier DH. For InAlAs-barrier DH, the larger experimental S than the calculated S implies the minor existence of trap-induced nonradiative recombination across the interface.

For InGaAs, the conduction band offset ΔEc for InP

Table 2 Calculated surface recombination velocity at barrier/InGaAsP interface using Eq..(3)

表2 采用公式(3)计算得到的背场/InGaAsP界面处的表面复合速率

Barrier	m_2 (m_0)	m_1 (m_0)	ΔEc (meV)	S (cm/s)
InP	0.08	0.047	230	5793
InAlAs	0.075	0.047	460	0.738

barrier and InAlAs barrier are 0.25 eV and 0.52 eV, respectively. The larger offset in conduction band means smaller thermionic emission velocity. Meanwhile, the valence band offset ΔEv for InP barrier and InAlAs barrier are 0.35 eV and 0.17 eV[11]. The smaller offset in valence band indicates lower potential barrier for majority-carrier. Therefore, InAlAs should be more promising BSF layer in solar cells.

Figure 4 displays the overall SIMS results for DH stacks, and Fig. 5 shows the PL decay curves for individual DHs. Extracted lifetimes are summarized in Table 3. It is obvious that zinc concentration in confined layers rises with increased thermal history from DH1 to DH3. The concentration in DH2 is about 1.0×10^{17} cm^{-3}, while the concentration in DH3 is about 2.0×10^{17} cm^{-3}, in spite of the type of barriers. This provides further evidence that both InP and InAlAs present similar ability to block zinc diffusion. Although there is a downward trend from DH1 to DH3, the effective lifetimes in InAlAs-barrier DHs are always longer than those in InP-barrier DHs. It suggests the surface recombination velocity is still dominated by thermionic emission process. With zinc concentration increasing to 1.0×10^{17} cm^{-3}, the bulk carrier lifetime τ_{bulk} in DH2 decrease to approximately 100 ns, according to Eq. 2. Therefore, the surface recombination velocity S increase to 434 cm/s and 221 cm/s, for InP-barrier DH2 and InAlAs-barrier DH2 respectively. Since the drop of band offset is the only cause for thermionic emission related increase of S, it is supposed that diffusion of major III-V element across the interface, which would lead to such shrink of band offset, occurs during the thermal treatment.

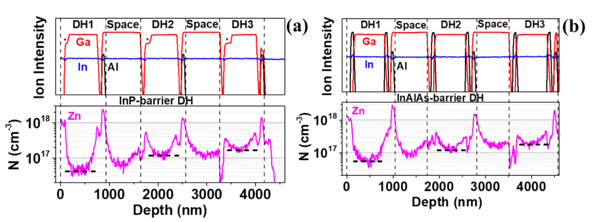

Fig. 4 Overall SIMS results of (a) InP-barrier DH stack and (b) InAlAs-barrier DH stack.

图4 InP双异质结(a)和InAlAs双异质结(b)的整体SIMS测试结果

As shown in Table 3, for DHs using the same type of barriers, the τ_{eff} in DH3 are quite close to the τ_{eff} in DH2. With zinc concentration of 2.0×10^{17} cm^{-3}, the bulk carrier lifetime τ_{bulk} in DH3 is approximately 50 ns, and S are 210.2 cm/s and 55.6 cm/s, for InP-barrier DH3 and InAlAs-barrier DH3 respectively. The abnormal decrease of S is probably due to the photon recycling effect, which leads to the longer τ_{eff} and smaller S in DH3 than expected.

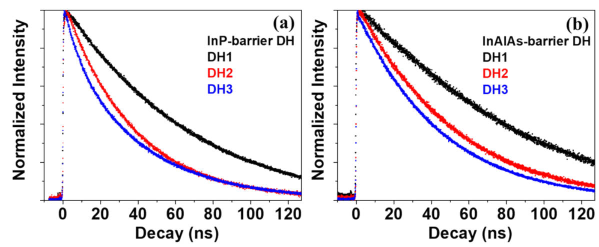

Fig. 5 PL decay curves of (a) InP-barrier DHs and (b) InAlAs-barrier DHs.

图5 InP双异质结(a)和InAlAs双异质结(b)的荧光发光衰减曲线

Table 3 The effective minority-carrier lifetime of the DHs

表3 双异质结的有效载流子寿命

τ_{eff} (ns)	DH1	DH2	DH3
InP-barrier	70.0	36.5	35.2
InAlAs-barrier	110.0	53.0	45.0

The steady-state PL of DHs confirms the above hypothesis. As shown in Fig. 6, the PL peak for DH1 and DH2 are of similar intensity, while PL intensities of DH3 are nearly one order of magnitude stronger. Considering the optical configuration of DH stack, the photon recycling is the most effective in DH3, and is suppressed in DH1 and DH2 due to extra absorption from underlying narrow bandgap InGaAs spacers.

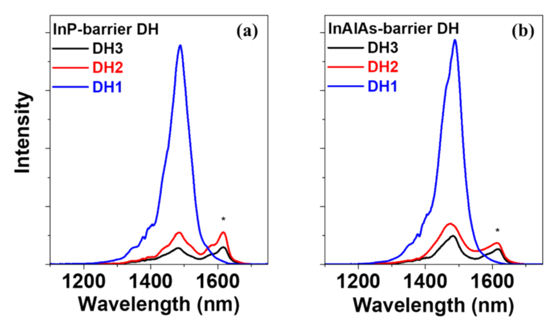

Fig. 6 Steady-state PL of (a) InP-barrier DHs and (b) InAlAs-barrier DHs. Weak peaks marked by asteroids in DH1 and DH2 are related to the spacers.

图6 InP双异质结(a)和InAlAs双异质结(b)的稳态荧光发光曲线。标*的微弱发光峰与背场相关

The results of InGaAsP/InGaAs DJSCs using both InP and InAlAs BSF layers confirm the advantages and effectiveness of InAlAs BSF layer in practical device. Figure 7 shows light J–V and EQE measurements of the devices. Using InAlAs BSF layer, the cell presents an efficiency of 9.28% with a V_{oc} of 983.2 mV, a J_{sc} of 15.6 mA/cm^2 and an FF of 0.818. Meanwhile, the device using InP BSF present a V_{oc} of 967.7 mV, a J_{sc} of 15.3 mA/

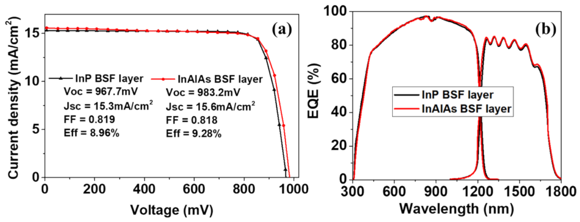

Fig. 7 (a) Light *J-V* and (b) spectra response curves for InGaAsP/InGaAs solar cells using InP and InAlAs BSF layers
图 7 采用 InP 和 InAlAs 背场的 InGaAsP/InGaAs 双结电池光照 *J-V* 曲线(a)和量子效率曲线(b)

cm^2 and an FF of 0. 819. An enhancement of V_{oc} is obtained, without any cost of J_{sc} and FF.

It is well established that SL serve as effective barrier for element diffusion or intermixing, and dislocation threading, and it has been widely used in semiconductor devices such as high electron mobility transistors, laser diodes, electro absorption modulators [12-16]. Also, the miniband in SL would not introduce extra potential barrier for carrier transport [17]. An initial five-period InP (2nm)/InAlAs(2nm) SL BSF layer is designed and employed in bottom InGaAs subcell of DJSC. A V_{oc} of 997. 5 mV, a *Jsc* of 15. 8 mA/cm^2 and an FF of 0. 824 are obtained as in Fig. 8. Both V_{oc} and Jsc are boosted, as expected, in fabricated SL BSF device. The V_{oc} approaches 1. 0 V, resulting in a Woc of 752. 5 mV. A reduction of 30 mV in V_{oc} loss for DJSC is achieved, compared with the conventional InP BSF DJSC.

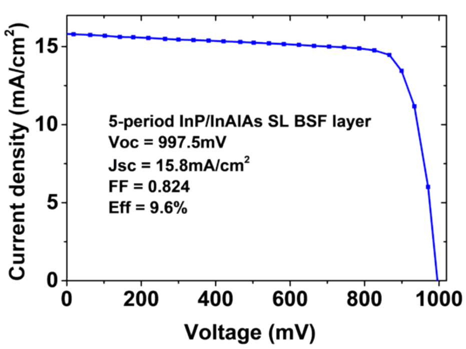

Fig. 8 Light J-V for InGaAsP/InGaAs DJSC using 5-period InP/InAlAs SL BSF layer.
图 8 采用 5 对 InP/InAlAs 超晶格背场的 InGaAsP/InGaAs 双结电池光照 J-V 曲线

3 Conclusions

In general, the use of novel SL BSF layer in the bottom subcell reduces the V_{oc} loss in InGaAsP/InGaAs DJSC.

Experiments show that, the mechanism of minority-carrier transport at BSF/base interface of the bottom subcell of InGaAsP/InGaAs DJSCs is dominated by thermionic emission, instead of defect-induced recombination, which is in contrast to previous reports. It also shows that both InP and InAlAs cannot prevent the zinc diffusion effectively. In addition, intermixing of major III-V element occurs as a result of increasing thermal treatment.

Based on the above results, an initial 5-period InP/InAlAs SL BSF layer is designed and employed in bottom InGaAs subcell of DJSC. A V_{oc} of 997. 5 mV, a J_{sc} of 15. 8 mA/cm^2 and an FF of 0. 824 are obtained. The V_{oc} approaches 1. 0 V, resulting in a W_{oc} of 752. 5 mV. A reduction of 30 mV in V_{oc} loss for DJSC is achieved, compared with the results of conventional InP BSF configuration. It suggests that such SL BSF would benefit the V_{oc} enhancement for four-junction solar cells.

References

[1] D. Frank, M. Grave, P. Beutel, *et al*. Wafer bonded four-junction GaInP/GaAs//GaInAsP/GaInAs concentrator solar cells with 44.7% efficiency[J], Prog. *Photovolt*: *Res. Appl.*, 2014, **22**: 277–282.
[2] R. Oshima, K. Makita, H. Mizuno, *et al.*, MBE–grown InGaAsP solar cells with 1.0 eV bandgap on InP (001) substrates for application to multijunction solar cells[J], *Japanese Journal of Applied Physics*, **2015**, 54: 14–14.
[3] Y. Wu, L. Ji, P. Dai, *et al*. Effects of buffer layer and back–surface field on MBE–grown InGaAsP/InGaAs solar cells[J], *Japanese Journal of Applied Physics*, 2016, **55**: 022301–4.
[4] Y. Zhao, J. Dong, K. Li, *et al*. InGaAsP/InGaAs tandem photovoltaic devices for four–junction solar cells[J], *Journal of Semiconductors*, 2015, **36**: 044011–4.
[5] R. R. King, D. Bhusari, A. Boca, *et al.*, Band gap–voltage offset and energy production in next–generation multijunction solar cells [J], *Prog. Photovolt*: *Res. Appl.*, 2011, **19**: 797–812.
[6] John Briceet al., *Properties of INDIUM PHOSPHIDE*, [C] INSPEC, EMIS Data reviews Series, 1991, **6**: 280–281.
[7] Lu H, Li X, Zhang W, *et al*. MOVPE grown 1.0 eV InGaAsP solar cells with bandgap–voltage offset near to ideal radiative recombination limit[J]. *Solar Energy Materials and Solar Cells*, 2019, **196**: 65–69..
[8] Boulou M, Bois D. Cathodoluminescence measurements of the minority-carrier lifetime in semiconductors[J]. *Journal of Applied Physics*, 1977, **48**(11):4713–4721.
[9] R. K. Ahenkiel, M. S. Lundstrom, Minority Carriers in III–V Semiconductors: Physics and Applications, Semiconductors and Semimetals[J], *Academic Press*, *Inc.*, 1993, **39**: 57–59.
[10] D.Schroeder, *Modelling of Interface Carrier Transport For Device Simulation*[M], Spinger, 1994, 166.
[11] S. Adachi, *Physical Properties Of III–V Semiconductor Compound* [M], JOHN WILEY&SONS, 1992, 75–109.
[12] Ross R L, Svensson S P, Lugli P. Pseudomorphic HEMT Technology and Applications[M]. Springer Netherlands, 1996..
[13] Zhu D H, Wang Z G, Liang J B, *et al*. 808 nm high–power laser grown by MBE through the control of Be diffusion and use of superlattice [J]. *JOURNAL OF CRYSTAL GROWTH*, 1997, **175**: 1004–1008..
[14] Chelakara R V, Islam M R, Neff J G, *et al*. Growth of high–quality InAlP/InGaP quantum wells and InAlP/InGaP superlattice barrier cladding layers by metalorganic chemical vapor deposition[J]. *Journal of Crystal Growth*, 1994, **145**(1–4):179–186..
[15] Givens M E, Mawst L J, Zmudzinski C A, *et al*. Effect of compositionally graded and superlattice buffer layers on the device performance of graded barrier quantum well heterostructure laser diodes [J]. *Applied Physics Letters*, 1987, **50**(6):301–303.
[16] Zhang J, Chen X Y, Ma Y J, *et al*. Optimization of In0.6Ga0.4As/InAs electron barrier for In0.74Ga0.26As detectors grown by molecular beam epitaxy[J]. *Journal of Crystal Growth*, 2019, **512**:84–89.
[17] John H Davis, *The Physics of Low–Dimensional Semiconductors*[M], Cambridge University Press, 2005: 177–182.

第10届国际应用光学与光子学技术交流大会会议论文征文通知

https://www.csoe.org.cn/meeting/AOPC2021/
2021年6月20–22日 北京国家会议中心(CNCC)
主办单位: 中国光学工程学会(CSOE)、SPIE
大会主席: 张广军 (东南大学)、Byoungho Lee (Seoul National University, Korea)
征文议题:
Topic1: Advanced Laser Materials and Laser Technology / 新型激光材料与激光器
Topic2: Advanced Laser Processing and Manufacturing / 激光先进制造与装备
Topic3: Laser Transmission and Communication / 激光传输与通信技术
Topic4:Laser field control and beam control /激光光场调控和光束控制
Topic5: THz Technology and Applications / 太赫兹技术
Topic6: Infrared Devices and Infrared Technology / 红外器件与红外技术
Topic7: Optoelectronic Devices and Integration / 光电子集成
Topic8: Nano Photonics / 微纳光子学
Topic9: Display Technology and Optical Storage / 先进显示技术与光存储
Topic10: Optical Display and Sensing in Augmented, Virtual, and Mixed Reality (AR, VR, MR) /增强、虚拟和混合现实(AR、VR、MR)中的光显示和光传感
Topic11: Optical Spectroscopy and Imaging / 光谱仪与光谱成像
Topic12: Optical Sensing and Imaging Technology / 光电探测与成像技术
Topic13: Novel Optical Design / 新体制光学设计
Topic14: Optics Ultra Precision Manufacturing and Testing / 超精密光学加工与检测技术
Topic15: Quantum Information Technology / 量子信息技术
Topic16: Micro-optics and MOEMS / 微光学与微光机电系统
Topic17: Biomedical Optics / 生物医学光子学
Topic18: Atmospheric and Environmental Optics / 大气与环境光学
Topic19: Optical Information and Network / 光信息与光网络
Topic20: Space Optics, Telescopes and Instrumentation / 望远镜、空间光学与仪器
Topic21: AI in Optics and Photonics / 人工智能在光学与光子学应用
发表须知:
会议论文由SPIE正式出版,EI核心收录。作者请登陆投稿网站先提交英文摘要(不少于500单词),大会学术委员会审查后,组委会用邮件给作者发录用通知。英文摘要截稿日期:2021年3月20日(第一轮)。
英文摘要投递网址:https://b2b.csoe.org.cn/submission/AOPC2021.html
支持期刊:
PhotoniX, Journal of Electronic Imaging (SCI) , Journal of Applied Remote Sensing (SCI), Optical Engineering (SCI), Journal of Micro/Nanolithography, MEMS, and MOEMS (SCI) , Photonic Sensors (SCI) , Journal of Infrared and Millimeter Waves (SCI), Infrared and Laser Engineering(Ei), Acta Photonica Sinica(Ei), International Journal of Extreme Manufacturing, SPIE Proceedings(Ei), etc.
秘书处:
刘艳,liuyan@csoe.org.cn,022-58168510
蔡方方,cai_ff@csoe.org.cn,022-58168541